

# Direct Observation of Coronal Magnetic Fields by Vector Tomography of the Coronal Emission Line Polarizations

M. Kramar<sup>1</sup>, H. Lin<sup>2</sup>, S. Tomczyk<sup>3</sup>

<sup>1</sup>*Physics Department, The Catholic University of America, 620 Michigan Ave NE, Washington, DC 20064*

<sup>2</sup>*Institute for Astronomy, University of Hawaii at Manoa, 34 Ohia Ku Street, Pukalani, Maui, HI 96768*

<sup>3</sup>*High Altitude Observatory, 3080 Center Green Drive, Boulder, CO 80301*

## ABSTRACT

This article presents the first direct “observation” of the global-scale, 3D coronal magnetic fields of Carrington Rotation (CR) Cycle 2112 using vector tomographic inversion techniques. The Vector tomographic inversion uses observational measurements of the Fe XIII 10747 Å Hanle effect polarization signals by the Coronal Multichannel Polarimeter (CoMP) and coronal density and temperature structures derived from scalar tomographic inversion of STEREO/EUVI coronal emission lines (CELs) intensity images as inputs to derive a coronal magnetic field model that best reproduces the observed polarization signals. While independent verifications of the vector tomography results cannot be performed, we compared the tomography inverted coronal magnetic fields with those constructed by MagnetoHydroDynamic (MHD) simulation based on observed photospheric magnetic fields of CR 2112 and 2113. We found that the MHD model for CR 2112 is qualitatively consistent with the tomography inverted result for most of the reconstruction domain except for a couple of regions. Particularly for one of the most noticeable exception region, we found that the MHD simulation for CR 2113 predicted a model that more closely resemble the vector tomography inverted magnetic fields. We discuss the utilities and limitations of the tomographic inversion technique, and present ideas for future developments.

*Subject headings:* Sun: corona — Magnetic fields — Sun: infrared

---

<sup>1</sup>e-mail: kramar@cua.edu

## 1. Introduction

Routine direct measurements of the coronal magnetic fields are indispensable for our eventual understanding of the nature of solar coronal phenomena at all spatial and temporal scales. Important progresses were made in the last two decades in the development of the theories (Casini & Judge 1999; Lin & Casini 2000; Casini & Lin 2002), instrumentation and observing techniques (Lin et al. 2000, 2004) to directly measure the polarization of coronal emission lines (CELs) that bear the information of the coronal magnetic fields. A major milestone was reached with the deployment of the Coronal Multichannel Polarimeter (CoMP, Tomczyk et al. 1995, 2007). CoMP provides synoptic linear polarization measurements of the Fe XIII 10747 Å emissions which directly maps the orientation of the magnetic fields of the solar corona. However, due to the low density and opacity of the coronal atmosphere the observed polarization signals are the total signals summed along the line-of-sight (LOS) of the measurements with non-uniform temperature, density and magnetic field structures. Therefore, except in a few special cases, direct inference of the 3D coronal magnetic field structure from polarization data is in general not possible.

Parallel to the development of the observing capabilities, a vector tomography inversion method to infer the coronal magnetic fields based on CEL circular polarization data was developed by Kramar et al. (2006). More recently a second vector tomography inversion method that combines coronal linear polarization data and information of the temperature and density structure of the corona to reconstruct the 3D coronal magnetic fields was developed by Kramar et al. (2013). We applied this technique to CoMP data obtained during Carrington Rotation (CR) cycle 2112 to derive the global 3D coronal magnetic fields above the east limb of the sun. However, as it was pointed out in Kramar et al. (2013), while polarizations of the CELs respond directly to the local magnetic fields, their visibility, i.e., the strength of the emission lines, strongly depends on local thermodynamic properties of the plasma. Therefore, 3D temperature and density structures of the corona are also needed as inputs for the vector tomographic inversion program for the calculation of the strength of the coronal emission lines. In this work the 3D temperature and density structure of the corona were derived by scalar tomographic inversion of the EUVI coronal images obtained by the STEREO/EUVI instrument. In the following sections, we will first describe the scalar inversion we used to derive the temperature and density distribution of the corona from STEREO/EUVI data. Then we will present results from the vector tomographic inversion of the 3D magnetic fields of CR 2112. Limitations of this methods, as well as future improvement of the technique will be discussed.

## 2. Reconstruction of Density and Temperature

The technique for the 3D reconstruction of the density and temperature of the corona is similar to the Differential Emission Measure Tomography (DEMT) method described by Vásquez et al. (2010). The main difference between these two techniques is that, in our method, we assumed the plasma is isothermal within each volume element (voxel). Briefly, the measured coronal emission  $I_\lambda$  in any of the EUVI channels can be represented by the LOS integral

$$I_\lambda = k \cdot \int_{\text{LOS}} \varepsilon_\lambda(\vec{r}) d\ell, \quad (1)$$

where  $\varepsilon_\lambda(\vec{r})$  is the emissivity at the position  $\vec{r}$  in the corona for the selected channel  $\lambda$ , i.e., light intensity (in photons per second) emitted per unit volume, per unit solid angle. The coefficient  $k$  accounts for pixel size, aperture, distance to the Sun. The inversion of 1 for  $\varepsilon_{171}(\vec{r})$ ,  $\varepsilon_{195}(\vec{r})$ , and  $\varepsilon_{284}(\vec{r})$  is performed by tomography method described in Kramar et al. (2014).

For an locally isothermal plasma,  $\varepsilon_\lambda(\vec{r})$  can be expressed by (Phillips et al. 2008)

$$\varepsilon_\lambda = G(T, N_e) N_e^2, \quad (2)$$

where  $T$  is the temperature,  $N_e$  is electron density (and a function of  $T$ ), and  $G(T, N_e)$  is the contribution function. For our inversion  $G(T, N_e)$  was calculated with the CHIANTI code (Dere et al. 2009), and the Fe ions abundances were derived from results of Arnaud & Raymond (1992). For every grid cell, we derive three (one for each EUVI channel)  $N_e(T)$  curves from (2) based on the emissivities  $\varepsilon_\lambda(\vec{r})$  derived by the tomography from equation (1). With the local isothermal approximation, the three  $N_e(T)$  curves will converge at a point indicating the solution for  $T$  and  $N_e$  for a given grid cell.

We applied this inversion method to the STEREO/EUVI (Wuelser et al. 2004; Howard et al. 2008) data of CR 2112. STEREO/EUVI observes the coronal up to approximately  $1.7 R_\odot$  in four spectral channels (171, 195, 284, and 304 Å). We used the off-limb data of images from the 171, 195, and 284 channels for the tomographic inversion of the temperature and density. Similarly to Vásquez et al. (2010), three average images per channel per day over half a solar rotation during CR2112 were used for the reconstruction. The average images were obtained by averaging three off-limb images taken with a two hours interval. The resolution of the EUVI images were also reduced to  $512 \times 512$  for the reconstruction. The reconstruction domain was limited to  $1.5 R_\odot$  due to the lower signal-to-noise ratio of data higher in the corona. Figure 1 shows a spherical cross-section of the reconstructed 3D electron density and temperature for CR 2112 at  $1.1 R_\odot$ .

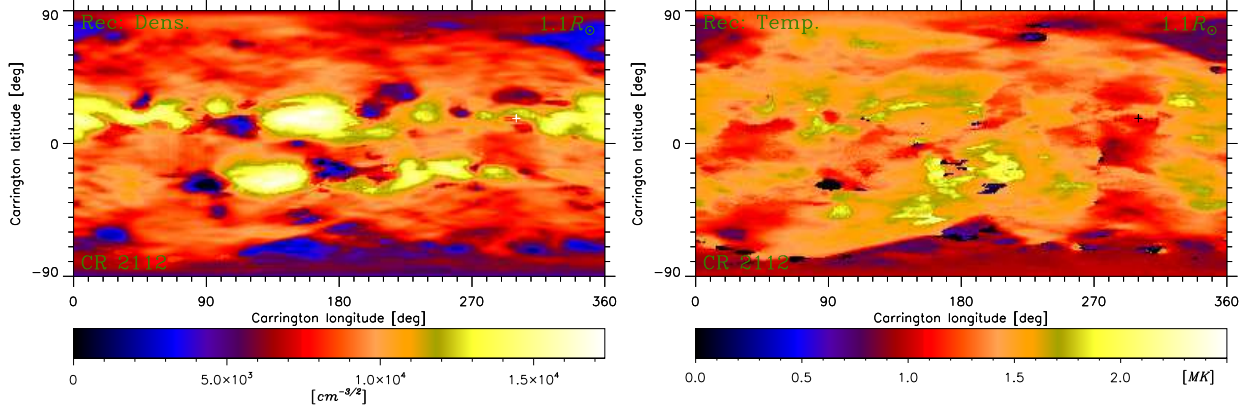


Fig. 1.— Spherical cross-section of the reconstructed 3D electron density (left) and temperature (right) at heliocentric distance of  $1.1R_{\odot}$ .

### 3. Reconstruction of Magnetic Fields

The CoMP instrument measures the intensity and the linear and circular polarization (Stokes I, Q, U, V) of the Fe XIII lines at 10747 and 10798 Å of the solar corona from  $\sim 1.03$  to  $\sim 1.4R_{\odot}$ . In present research, we use data only for the 10747 Å forbidden line. Averaged daily CoMP Stokes  $Q$  and  $U$  images from July 13 to July 26, 2011, corresponded to CR 2112, are used for this study. The reconstruction of the coronal magnetic fields follows the method described in Kramar et al. (2013), using the 3D  $T_e$  and  $N_e$  derived from tomographic inversion of STEREO/EUVI data as fixed input parameters. Although  $T$  and  $N_e$  were derived out to  $1.5R_{\odot}$ , examination of the results indicated that the inversion above  $1.3R_{\odot}$  may not be very reliable. Therefore the outer boundary of the reconstruction domain for the magnetic fields were limited to  $1.3R_{\odot}$  for this work.

Figure 2 shows the magnetic field lines originated at Carrington longitudes  $\pm 90^\circ$  from LOS directions of 110.5 and 205.5°. Figures for all cross-sections are available in the online supplementary material. The black lines represent reconstructed field lines derived from the vector tomographic inversion based on CoMP data, and the red dashed lines are field lines from MHD model (Mikić et al. 2007; Lionello et al. 2009)<sup>1</sup> used as the starting field for the inversion. Maps of the whole reconstructed 3D fields are shown in the on-line version of this paper.

The jagged appearances of some of the field lines in the reconstructed model can be attributed errors in 3D density and temperature reconstructions, the decreasing magnetic

---

<sup>1</sup>[www.preds-ci.com](http://www.preds-ci.com)

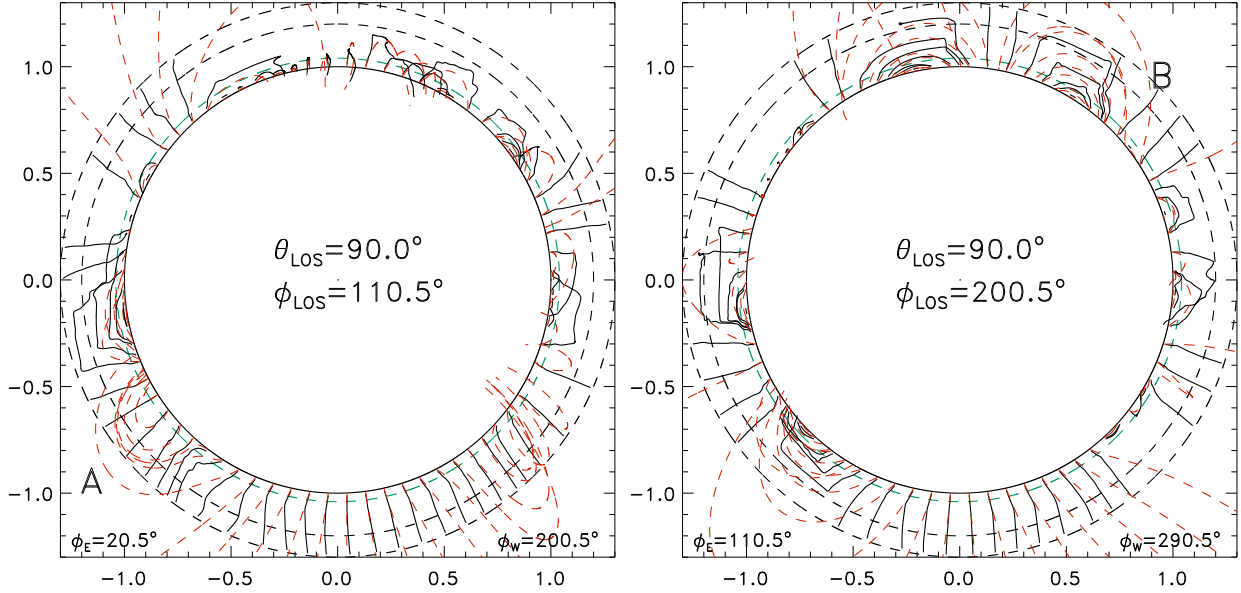


Fig. 2.— Magnetic field lines originated at Carrington longitudes  $\pm 90^\circ$  from LOS directions of  $110.5^\circ$  and  $205.5^\circ$ . Magnetic field lines of reconstructed coronal magnetic field (black) and MHD model (red) used as starting field. The fields are for CR 2112. Inner and outer dashed circles show input data coverage area. Middle dashed circle is located at  $1.2R_\odot$  and plotted just for reference purpose. The animation with a full set of Carrington longitudes is in electronic supplemental material.

field strength as a function of height which makes the regularization less effective at larger heliocentric distances, and reconstruction errors near outer boundary of the reconstruction domain due to limited field of view (FOV,  $1.3R_\odot$ ) of the input polarization data. Nevertheless, the reconstructed fields possess sufficient details to analyse the large scale structure of the coronal magnetic fields. It is interesting to note that the reconstructed fields are qualitatively similar to the starting fields except in the region above the south-east limb labelled **A** (or region **B** at Carrington longitude of  $290^\circ$ ), where the tomographic inversion resulted in an open field while the starting fields were in a closed configuration.

It should be stressed that currently it is impossible to perform independent verification of the tomographic inversion results — MHD models based on observed photospheric magnetic fields inputs were derived with an independent set of assumptions, and are subjects to its own limitations and uncertainties, and at this point which method provides more accurate result cannot be assessed. However, there are indirect observations that lend support to the accuracy of the tomographic inversion results. First of all, current sheet structures are known to be associated with closed dipole-like magnetic field structures as demonstrated

by Kramar et al. (2014). However, the 3D electron density structures of CR 2112 obtained by tomography of the STEREO/COR1 data (Kramar et al. 2009) as shown in Figure 4 shows no sign of current sheet. Secondly, we noticed that the photospheric magnetic fields used as the boundary condition of the MHD model that was used as our initial fields for inversion contains data collected about 3/4 solar rotation before the reference date of the region “A” CoMP observation, and may represent an older field configuration. Examination of the MHD model for the next CR 2113 as shown in Figure 3 reveals that it has a magnetic field configuration similar to that of the tomographic inverted results. These observations appear to suggest that both MHD simulations based on photospheric boundary conditions and tomographic inversion based on CEL polarization data are capable of yielding the large-scale coronal magnetic field structures, albeit they are subject to different uncertainties and possess different type of errors.

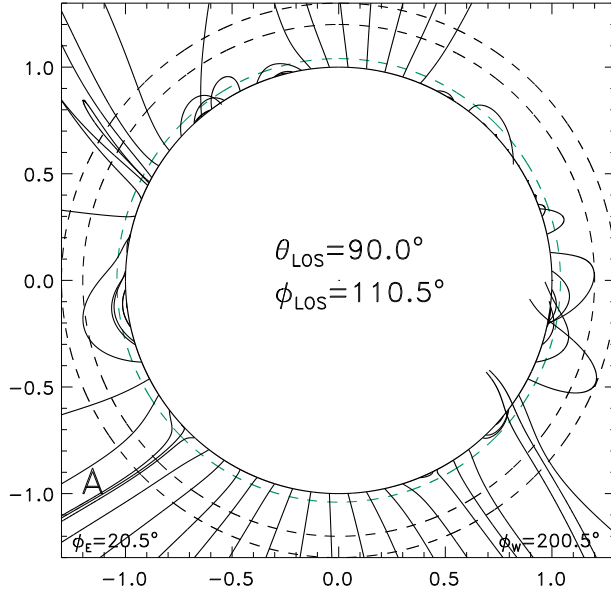


Figure 3 Magnetic field lines of the MHD model for CR 2113. Meridional cross-section for Carrington longitude of 20.5°.

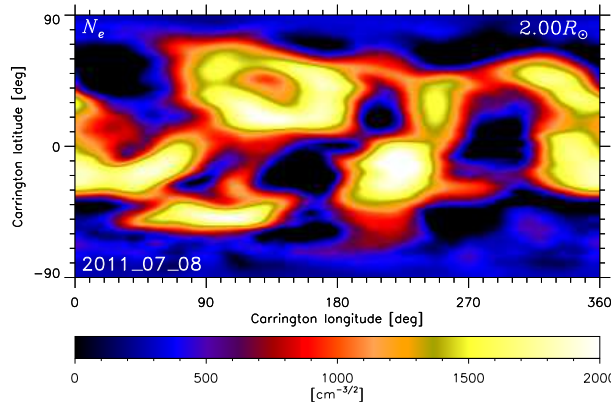


Figure 4 Spherical cross-section of the reconstructed electron density in square-root scale at heliocentric distance of  $2 R_{\odot}$ . The reconstruction is obtained by tomography based on COR-1 data obtained during July, 2011 (CR 2112).



#### 4. Discussions and Conclusions

We have performed the first “observation” of the 3D coronal magnetic field using a combination of vector tomographic inversion of IR CEL *linear* polarization data and scalar tomographic inversion of CEL intensity data in the UV wavelengths. We compared the tomography inverted coronal magnetic fields with those constructed by MHD simulation based on observed photospheric magnetic fields of CR 2112 and 2113. and with the global 3D coronal electron density structure obtained by tomography based on STEREO/COR1 data. This paper present a first look and preliminary analysis of the results. A comprehensive analysis of the 3D coronal fields and its relationship to the temperature and density structures, as well as comparison with other coronal models will be presented in a future paper.

Tomography requires simultaneous observations of the same object through multiple sight lines. While current instrumentation capabilities do not allow for simultaneous observation of the CEL polarization from more than one sight line, data obtained over an extended period of time as the sun rotates can be interpreted as data from multi-sight-line observations for stable, long-lived coronal magnetic field structures. On other side, the widely used global extrapolation methods such as global MHD, potential field, force-free field models use *photospheric* field data collected over a solar rotation period as a boundary condition (see Section 1 in Kramar et al. (2014) and references therein) while the tomography requires *coronal* observations during only a half of a solar rotation period. Therefore, the coronal magnetic field structures derived from this *vector tomography* inversion method should be fair representation of long-lived, large scale magnetic structures. Additionally, because our 3D tomographic reconstructions are based on *coronal* observations, their results can serve as test and/or as additional constraints for various coronal models.

This research utilizes polarization data from only one spectral line. To further improve the accuracy and reliability of this technique, we plan to incorporate additional polarization data from the Fe XIV 5303 Å line from the visible CoMP instrument at Lomnický Stit Observatory in Slovakia (Rybák et al. 2010). We also plan to include STEREO/EUVI on-limb data to improve the accuracy of the temperature and density inversion. Finally, the current vector tomographic inversion utilizes only CEL linear polarization data which only yield information about the direction of the magnetic field projected in the POS. As the sensitivity of the instruments continue to improve, incorporation of the CEL line intensity and circular polarization data that carry information about the height of the data sources, and the strength of the longitudinal component of the magnetic fields will further improve the accuracy and sensitivity of the vector tomographic inversion technique. Future projects, such as the Daniel K. Inouye Solar Telescope currently under construction on the summit of Haleakala (Elmore et al. 2014), or the Coronal Solar Magnetism Observatory (COSMO)

proposed by the High Altitude Observatory and its partners, will be able to provide the full-Stokes data for the full-vector tomographic inversion, leading to a more accurate 3D reconstruction of the coronal magnetic field.

### **Acknowledgment**

The authors would like to thank Phill Judge of the High Altitude Observatory for providing the CLE codes used to compute the emission coefficients of the Stokes I,Q,U and V parameters for the forbidden coronal emission lines. The National Center for Atmospheric Research is sponsored by the National Science Foundation (NSF). This research was supported by NSF National Space Weather Program grant number AGS0819971.

### **REFERENCES**

- Arnaud, M., & Raymond, J. 1992, *ApJ*, 398, 394
- Casini, R., & Judge, P. G. 1999, *ApJ*, 522, 524
- Casini, R., & Lin, H. 2002, *ApJ*, 571, 540
- Dere, K. P., Landi, E., Young, P. R., et al. 2009, *A&A*, 498, 915
- Elmore, D. F., Rimmele, T., Casini, R., et al. 2014, in *Society of Photo-Optical Instrumentation Engineers (SPIE) Conference Series*, Vol. 9147, *Society of Photo-Optical Instrumentation Engineers (SPIE) Conference Series*, 7
- Howard, R. A., Moses, J. D., Vourlidas, A., et al. 2008, *Space Sci. Rev.*, 136, 67
- Kramar, M., Airapetian, V., Mikić, Z., & Davila, J. 2014, *Sol. Phys.*, 289, 2927
- Kramar, M., Inhester, B., Lin, H., & Davila, J. 2013, *ApJ*, 775, 25
- Kramar, M., Inhester, B., & Solanki, S. K. 2006, *A&A*, 456, 665
- Kramar, M., Jones, S., Davila, J., Inhester, B., & Mierla, M. 2009, *Sol. Phys.*, 259, 109
- Lin, H., & Casini, R. 2000, *ApJ*, 542, 528
- Lin, H., Kuhn, J. R., & Coulter, R. 2004, *ApJ*, 613, L177
- Lin, H., Penn, M. J., & Tomczyk, S. 2000, *ApJ*, 541, L83



- Lionello, R., Linker, J. A., & Mikić, Z. 2009, *ApJ*, 690, 902
- Mikić, Z., Linker, J. A., Lionello, R., Riley, P., & Titov, V. 2007, in *Astronomical Society of the Pacific Conference Series*, Vol. 370, *Solar and Stellar Physics Through Eclipses*, ed. O. Demircan, S. O. Selam, & B. Albayrak, 299
- Rybák, J., Ambróz, J., Gömöry, P., et al. 2010, in *20th National Solar Physics Meeting*, ed. I. Dorotovic, 196–200
- Tomczyk, S., McIntosh, S. W., Keil, S. L., et al. 2007, *Science*, 317, 1192
- Tomczyk, S., Streander, K., Card, G., et al. 1995, *Sol. Phys.*, 159, 1
- Vásquez, A. M., Frazin, R. A., & Manchester, IV, W. B. 2010, *ApJ*, 715, 1352
- Wuelser, J.-P., Lemen, J. R., Tarbell, T. D., et al. 2004, in *Society of Photo-Optical Instrumentation Engineers (SPIE) Conference Series*, Vol. 5171, *Telescopes and Instrumentation for Solar Astrophysics*, ed. S. Fineschi & M. A. Gummin, 111–122